Feasibility study of dissimilar metal joining by laser riveting of Ti-6Al-4V to AA6061

Bowei Li, Ali Khan, Bin Wang, et al.

COLLECTIONS

Paper published as part of the special topic on Proceedings of the International Congress of Applications of Lasers & Electro-Optics (ICALEO® 2021))

open access

View Online   Export Citation   CrossMark

ARTICLES YOU MAY BE INTERESTED IN

Automatically controlled laser-based welding process for repair of CFRP parts
Journal of Laser Applications **34**, 012006 (2022); https://doi.org/10.2351/7.0000480

Effect of low-level laser therapy on neurorehabilitation: A narrative review
Journal of Laser Applications **34**, 011201 (2022); https://doi.org/10.2351/7.0000577

Effects of laser parameters on machining precision and quality of wave-permeable materials
Journal of Laser Applications **34**, 012001 (2022); https://doi.org/10.2351/7.0000402

Feasibility study of dissimilar metal joining by laser riveting of Ti-6Al-4V to AA6061

View Online   Export Citation   CrossMark

Bowei Li,[1,2] (ID) Ali Khan,[3] Bin Wang,[1] (ID) and Paola De Bono[3]

AFFILIATIONS

[1]National Structural Integrity Research Centre, Granta Park, Cambridge CB2 16AL, United Kingdom
[2]College of Engineering, Design and Physical Sciences, Brunel University London, Kingston Lane, Uxbridge, Middlesex UB8 3PH, United Kingdom
[3]TWI Ltd., Granta Park, Cambridge CB21 6AL, United Kingdom

ABSTRACT

Aluminum of cylindrical profile (of diameter 1–4 mm) was trailed by laser metal wire deposition for potential riveting applications. The rivet was built onto a Ti6Al4V substrate through a hole in an AA6061 sheet. The built feature was postprocessed by a high-frequency laser washing technique to obtain the desired finish. Parameter optimization has allowed increased productivity by almost seven times while achieving required wetting conditions and metallurgical properties. It is found that the quality (both morphology and metallurgy) of the laser rivet joint is highly dependent on the laser wash parameters. The rivet crown and welding areas improved by the postwash process were directly reflected in the microhardness and shear tests and increased by 90% and 62%, respectively, compared with those in an unwashed rivet.

Key words: laser metal wire deposition, dissimilar joining, titanium, laser riveting

I. INTRODUCTION

In the aerospace and automotive sectors, lightweight structures are increasingly needed to reduce material use and energy costs. The dissimilar joining technology is one of the available options to achieve the goal of lightweight structures and material saving.[1,2] Titanium and aluminum have the advantage of excellent corrosion resistance and offer lightweight benefits, and their joining has been increasingly used in the aerospace industry.[3] However, in the fusion processing for aluminum and titanium joining, there remains a metallurgical difficulty. Research conducted has shown that numerous brittle intermetallic compounds may be formed in the thermal process, which weaken the mechanical strength of the joint.[4–6] Therefore, different processes for joining dissimilar materials have been developed, including friction stir welding,[7] riveting by mechanical fastening,[8] and adhesives.[9] For dissimilar joining of aluminum and titanium, mechanical fastening and adhesives are mature methods with high efficiency and lightweight merits,

but they still face the challenges of substrate penetration issue (in riveting) and working condition requirements (in adhesives).[10]

Additive manufacturing (AM) is a promising technology that can efficiently manufacture complicated components compared with traditional subtractive manufacturing. Among the many popular additive manufacturing methods, the powder bed fabrication process can produce complex parts precisely, and it is hard to manufacture large metal components and structures.[11,12] Directed energy deposition (DED) methods feed and deposit materials by energy sources like lasers, arc plasma, and electron beams. Depending on the feedstock formation, laser metal deposition is further classified into laser powder deposition (LPD) and laser metal wire deposition (LMWD). As comparative methods, because of the high accurate benefits of microfeedstock size and track of manufacturing systems, LPD can provide higher accuracy in processing control. However, previous research revealed that due to the shielding issue in the powder deposition process, LPD for Ti6Al4V

deposition increases contamination risks, which will significantly weaken the mechanical performance of fabricated structures. LMWD offers the benefits of enhanced deposition quality and mass input rate regarding the solid wire feeding form.[13,14] Therefore, LMWD is the preferable technique to manufacture the titanium components in AM.

In recent research for LMWD, the metallurgical and mechanical properties in a parametric study of Ti6Al4V single layer deposition were investigated,[15] and macrocurve track deposition in macroscales was explored and reported.[16] For multilayer LMWD research, hollow cylinders and cones were built in a macroscale (8–35 mm).[17] However, most laser deposition processing systems are equipped with a lateral wire feeder, resulting in the angle issue when building up the cylindrical feature in a minor scale.[18] Other studies investigated depositions of dissimilar materials.[19,20] Most of them used powders as the feeding material and built up multimaterial components with no joint.

The laser riveting (LR) concept is illustrated in Fig. 1 and further experimental detail is explained later in Fig. 4. In this work, a laser metal wire cylinder deposition (LMWCD) process was developed as a feasibility study to deposit a cylindrical feature in a minor scale, and three optimized methods [i.e., normal, high speed (HS), and continuous spiral (CS)] were investigated in a parametric study. Multilayer depositions were compared for productivity and metallurgical analysis. Based on this, LR as a new process was tried for depositing a Ti6Al4V wire through the hole in the upper AA6061 sheet onto a substrate plate of Ti6Al4V. A subsequent laser postscanning on the top of the deposited cylinder helped achieve a proper crown and welding condition. The geometrical appearance was observed and the rivet cross section was analyzed from microstructural aspects.

II. EXPERIMENT

A. Material and system setup

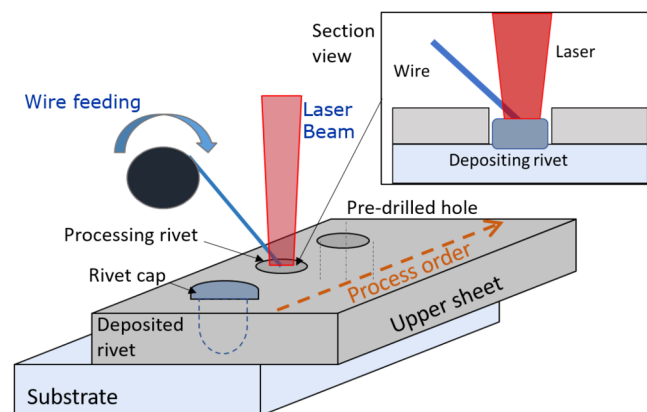In this work, the purpose of this trial study is to bind an upper aluminum sheet with a lower titanium sheet with deposited rivets by LMWCD (Fig. 1). Ti6Al4V (grade 5) alloy was used as the wire and substrate material, and AA6061 alloy as the upper sheet. The diameter of the wire is 0.8 mm, and the wire feed speed (WFS) and duration were automatically controlled and fed by the Binzel wire feeding system. The substrate and upper sheets were 4 and 2 mm, respectively.

The LMWCD processing system setup is shown in Fig. 2(a). The power source was a four-AXIS ytterbium fiber laser with 600 W maximum power (YLS-1000, IPG Photonics Corporation). The LMWD system was based on (1) the wire feeding device (driving unit and tube) with the wire nozzle being kept at 30° feeding angle to the substrate surface; (2) for the optical condition, the focus lens is 100 mm and the collimator is 200 mm, and the fiber diameter is 0.05 mm; (3) the laser head mounted on the motion system controlled by a computer numerical control (CNC)-system with the processing route predefined by programming; (4) the trailing shielding device, using argon (gas flow at 25 l/min) to protect the titanium welding pool from the oxidation and contamination.

B. LMWCD design

Very limited information can be found in open literature for producing a cylindrical profile on a minor scale. The basic additive layer manufacturing (ALM) method was thus adopted in circular deposition, as shown in Fig. 2(b). However, because the angle

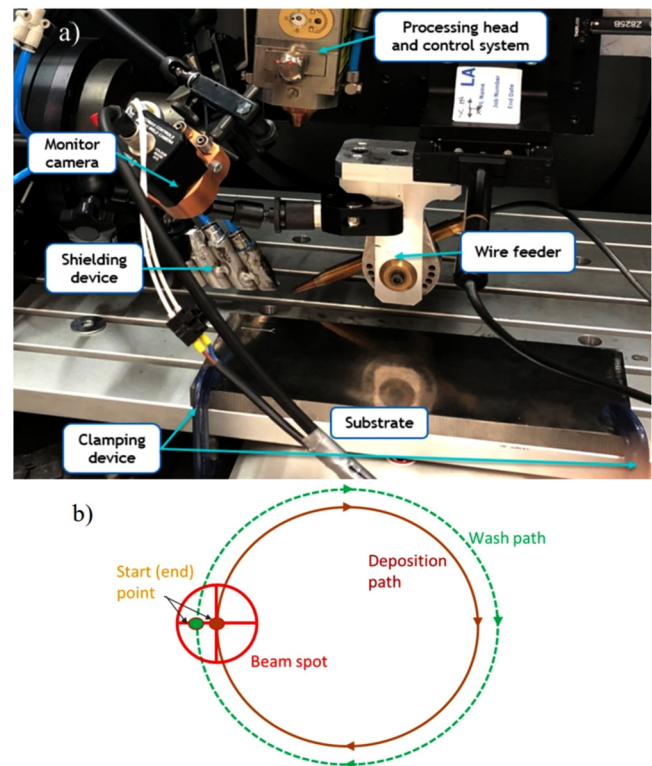FIG. 1. Schematic of the laser riveting concept.

FIG. 2. Experimental setup and methodology: (a) LMWCD processing system and (b) circular deposition path strategy in the feasibility study.

between the laser scanning and the feeding wire kept changing during the circular processing, the material was not uniformly melted and deposited. To solve this problem, a laser scanning wash path was added after deposition [Fig. 2(b)], leading to the spreading flow of the melt material over the target area. This also helped us to remove defects such as porosity and small cavities inside the deposition. The geometrical appearances, microstructure, and microhardness evaluations of the multilayer deposition produced are discussed later in Sec. III of this paper.

The duration of the processing time is one of the significant factors for potential industrial application, which directly influences efficiency and cost for the manufacturer. A further study aiming to reduce the total processing time for LMWCD was carried out with three different deposition strategies being developed in a parametric study. The circular path deposition was used as the initial control strategy named as the normal method (NM). Based on the normal method, an HS deposition method was designed to reduce the total processing time. The deposition and wash path speeds were doubled, and the cooling time between the deposited layers was reduced by half. A high-speed spiral (HSS) method was also designed. Still using the CS method (Fig. 3), the HSS process starts from the substrate and continues depositing the wire without a break until the final layer reaches the required height. This saved time from cooling steps and the wash path compared with ALM (NM and HS). The laser head is an IPG D30 welding head, and the 1.6 mm defocus beam spot is applied in the conduction welding mode; the setting of the processing parameters in all three deposition methods is listed in Table I.

C. LR procedures

The HSS deposition method was applied in the laser riveting concept; a titanium mushroomlike feature was to be built through the hole in the upper AA6063 sheet to interlock the substrate and the joint sheet. The diagram of LR procedures and processing positions is shown in Fig. 4. Because of the obstacle issue between the wire feeding angle and the size of hole (~4 mm diameter), the wire tip position had to be put at an offset height against the substrate, and the wire was kept at constant feeding in the first couple of seconds to build up the base additive layer and was continued with the spiral deposition. Following this, a high-frequency laser scanning (450 W, 0.3 mm beam spot, 4 mm scanning diameter circle with 200 Hz frequency) named postwash procedure was implemented by the IPG D30 wobbling function, on the top of deposition for 12 s to improve the joining condition and geometrical shape of the deposited rivet. Deposited rivets without and with postwash were compared, and their cross sections were evaluated by microstructure analysis and microhardness tests.

III. RESULTS

A. LMWCD feasibility study

Four-layer cylinder-shaped depositions were built by the circular path strategy using the additive layer method, as shown in Fig. 5(a). The wash path implemented at the end of each layer led to melted liquid spread over the surface of the deposited feature, providing a proper shielding finish. The finished rivets were cut, polished, and etched for microscopy (OM, Leica DMR) and SEM observation.

Ti6Al4V alloy contains hcp structure α and bcc structure β phases. They are commonly stabilized by aluminum and vanadium, respectively; depending on the heat treatment for the material, the phase change occurs and influences the mechanical performances of the alloy microstructure.[21] The microstructure map of the cross section of the finished deposit is shown in Fig. 5(b). Depending on the influence of the thermal history and phase transformation in
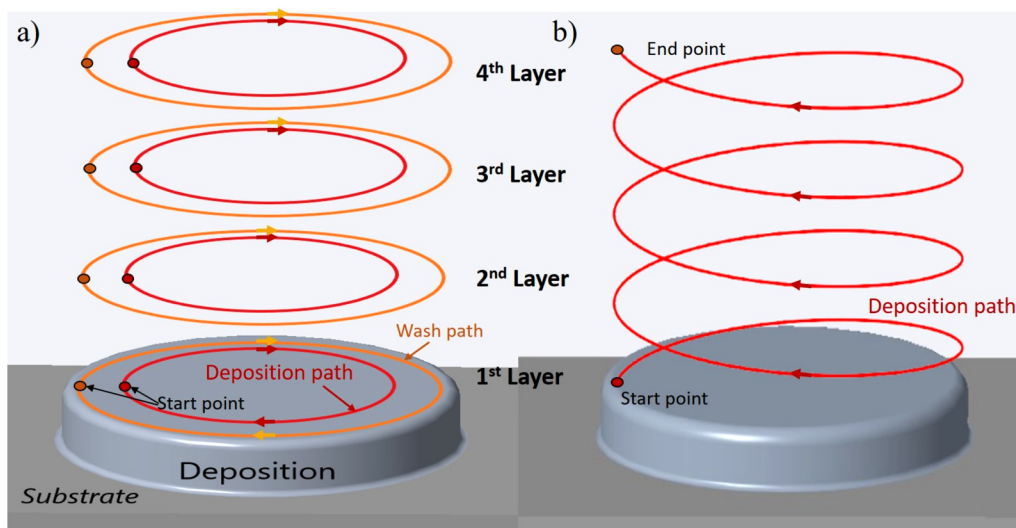

FIG. 3. Designed LMWCD methods in the parametric study: (a) ALM deposition method and (b) CS deposition method.
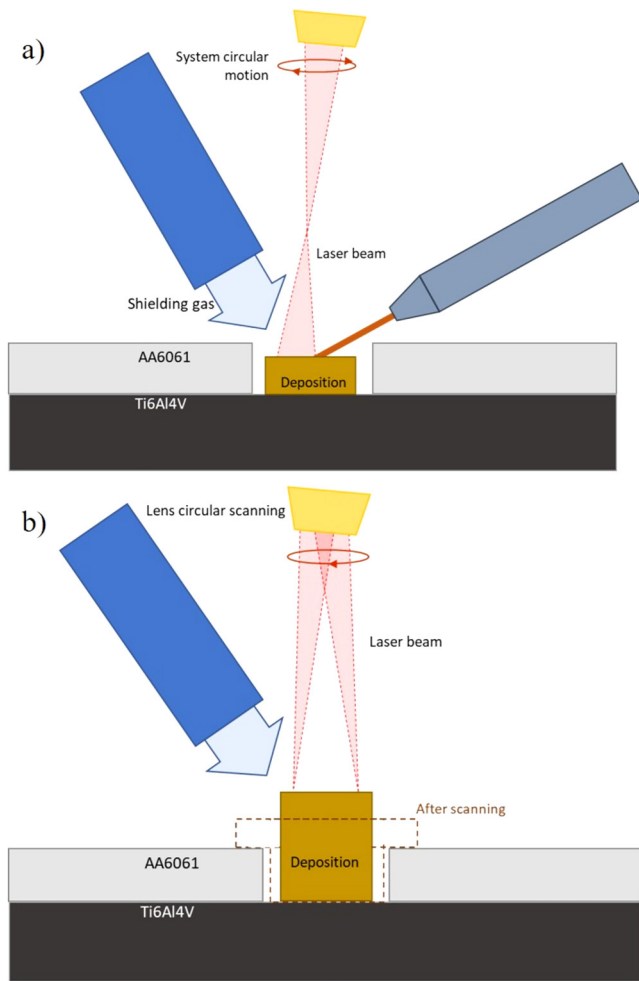
FIG. 4. Diagram of the LR processing: (a) rivet deposition and (b) high-speed laser postwash.

the process, the cross section is divided into three basic microstructure zones: the base material (BM), the heat-affected zone (HAZ), and the fusion zone (FZ) with added material (AM). This is in agreement with previous research using straight-line LMWD for single and multiple layer depositions.[14,22] The dissolution

TABLE I. Processing parameters of LMWCD and LR methods.

Deposition method	NM	HS	HSS	LR
Power range (W)		300–600		600
WFS (mm/s)	4.1	7.2		17
Deposition travel speed (mm/s)	0.75	1.5	1.5–3	2
Wash path speed (mm/s)	1.5	3		NA
Cooling gap (s)	8	3		

temperature T_{Diss}, approximately 708 °C as suggested in Ref. 23, is the starting point of the transfer from α-dissolution to β grains under equilibrium heating conditions and is classified by the peak temperature the substrate material undergoes. In HAZ, part of α dissolves into β grains, and in the upper area of the zone, the temperature was above the β-transus point and globular prior β grains were formed. In the fusion and added material zones, all materials were melted during the process, and columnar β grains were characterized. Acicular, Widmanstätten, and basket-weave structures can be observed in higher magnification.

Further grain detail was attained in the 200 times magnification photo taken by an optical microscope; the heat accumulation and cooling rate differences reflected on the middle columnar β grain and top equiaxed β grain areas are shown in Figs. 5(c) and 5(d), respectively. At the middle position, the relatively fast cooling condition occurred under the heat transfer from the base substrate, and the acicular α thus formed and refined by the repeat thermal cycles in the deposition and washing processes. However, in the top layer area, the last layer wire was melting on the deposited heated cylinder feature, and the temperature reaches the peak point and then slowly decreases to the room temperature under the air cooling condition, which led to the primary boundary and colony α grains generation. The above results show a high agreement with Ref. 24, which recorded the similar grain transmission phenomena in the macroscale straight-line LMWD, and revealed the α in various cooling conditions.

In addition, equiaxed β grains and a segregation band were formed in the last layer deposition, mainly because of the adjustment of power reduction and the thermal cycle. Due to the occurrence of remelting and annealing in the vertical area of the multiple layer DED, along with the decrease of heat effect from the melting pool, the segregation bands normally appear after the four-layer deposition in the processes of thin-walled LMWD and wire-arc additive manufacturing according to Refs. 25 and 26. In this riveting work, in order to control the deposition and solidification behavior to achieve a higher height, the deposition and wash path power inputs were reduced from 450 to 300 W in the third and fourth layers, respectively. It caused the early formation of segregation bands between the third and fourth layers, and the segregation curve clearly reflects that higher temperature went through the outer circular path. On the other hand, the lower heat input also led to a faster solidification, and the wash path only partly remelted the deposited material on the surface; thus, the liquid was of help on the top of the deposition to build a higher feature with a more desirable aspect ratio.

As seen in Fig. 5(b), no major defects such as pores and cracks were observed in the cross section. To evaluate the strength of the deposit, a microhardness test (Vickers) was carried out on the etched cross section with a 0.1 kg (HV0.1) force, and the result is shown in Fig. 6. The highest hardness (597) was measured in the final layer, where the material was deposited in the last track with the martensitic formation following a rapid cooling ratio. The segregation bands that underwent repeated thermal cycles attained higher hardness, while the rest of the AM and HAZ zones were hardened by solid solution, dislocation, and boundary hardening, which also increased the hardness compared to the BM.[27]
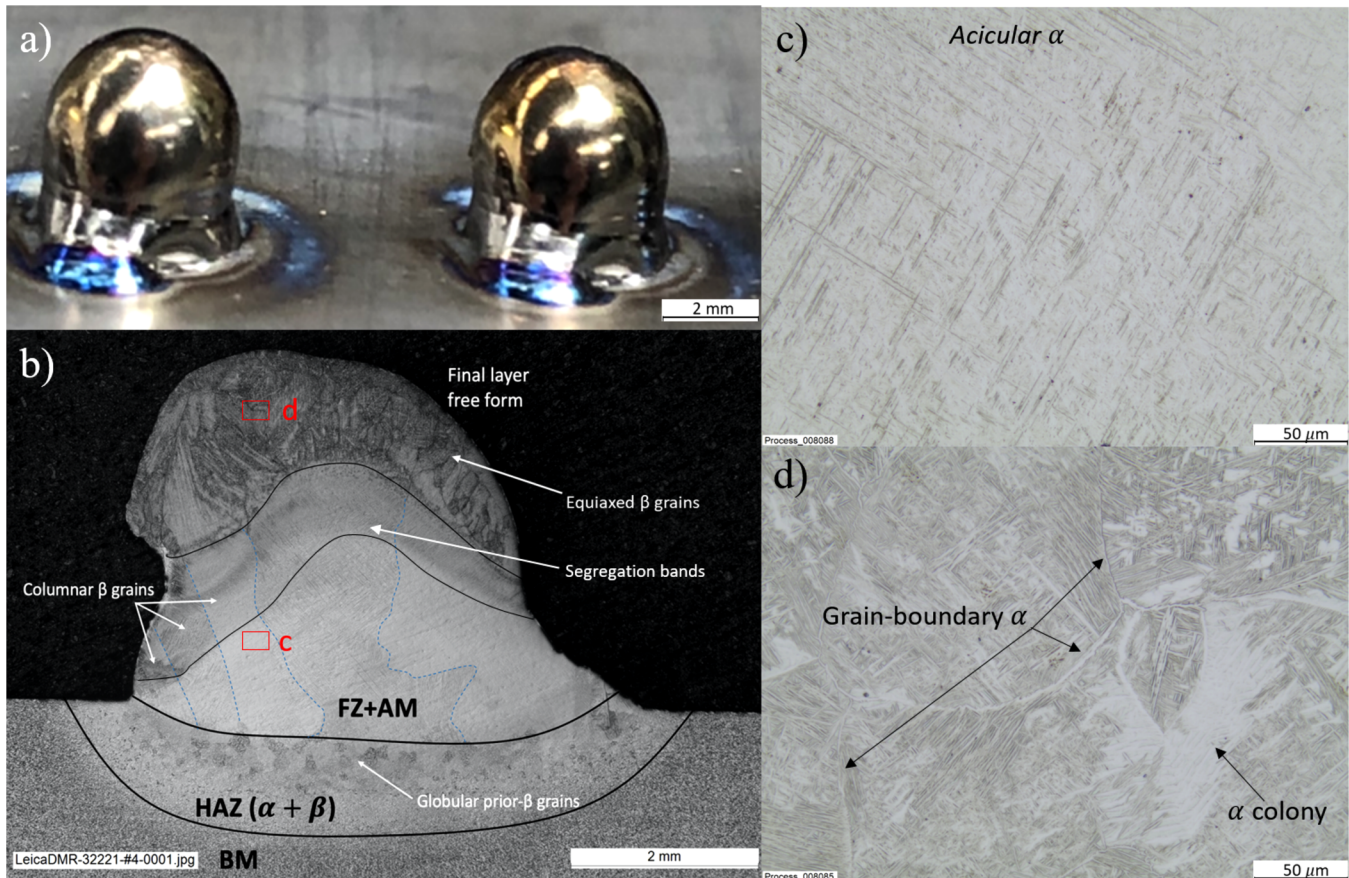
FIG. 5. Four-layer cylinder deposition built by additive layer method: (a) outlook of the cylinder feature; (b) microstructure map of the cross section; and the detail microstructure in the (c) middle and (d) top areas.

B. LMWCD parametric study

In order to increase the height of the cylinder deposit, trials of six-layer depositions by NM, HS, and HSS were carried out. Figure 7(a) shows the processing time of the three methods, taking from 87 s to build up a xi-layer deposition by NM to 38 s by the HS with a 56.3% reduction, and further to 13 s by HSS, at an 85.1% reduction in time and 6.7 times productivity compared to the original normal deposition method.

For the geometrical dimensions of depositions fabricated by different methods, although the wire feed speed was increased by the HSS method, the wire deposition time was much shorter than NM and HS processes. The expected deposition volume (V_{exp}) of HSS was still less than the other two methods. However, there was only little change in the geometrical dimensions of these three depositions. Due to the power reduction and higher motion speed, the energy accumulation in HSS was lower than that of HS. A faster solidification led to a higher built feature for the HSS process. On contrary, heat accumulation prevented the deposition

height growth in HS for the short cooling time in the layer gaps, resulting in a lower height and higher aspect ratio of the deposition.

The corresponding outlooks of the deposits can be seen in Fig. 7(b), the normal deposition shows the same microstructure with feasibility results in Fig. 7(c), and the cross section overviews of HS and HSS were presented in Figs. 7(d) and 7(e), respectively. Both of them obtained the intact section without the significant defects of pores and cracks, which normally occurred in the welding area. In addition, because these three deposition methods were all designed from the general layer additive manufacturing (LAM) concept, their macrostructure section overviews consisted with similar structures, the equiaxed β, columnar β, and globular prior β grains were observed in order from top to the weld areas. However, still some detailed differences were observed; the segregation band shows a strong relationship with the layer cooling steps, and the HS deposition shows a wider area of segregation bands since the faster thermal cycles and subsequent cooling gaps. On the contrary, only one narrow band is generated in the HSS deposition
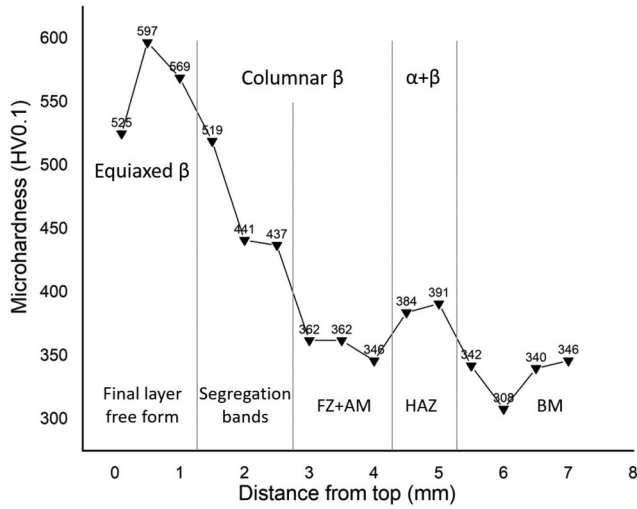
FIG. 6. Microhardness profile measured at the cross section of four-layer cylinder deposition.

regarding the continuous deposition process, and it also causes a higher heat accumulation and faster cooling rate inside, which increased the β grain size and reduced its number.

C. LR results

A number of rivets were made by the HSS method for joining between the Ti6Al4V substrate and the AA6061 sheet. Due to the restriction of the hole size and the feeding angle, wire feeding is started from a certain offset height, which limited the wetting and welding area between the deposition and substrate. Therefore, to improve the feature, a laser postwash procedure was carried out after the rivet deposition. Figure 8 illustrates the processing of LR deposition and postwash. Same as HSS cylinder deposition, a defocused laser was released onto the left side of the substrate in the hole and continued melting the surface to create a proper wetting condition for wire deposition [Fig. 8(a)]. Once the feeding wire was deposited onto the substrate and the first layer was established, the HSS strategy was executed by the CNC system to build up a six-layer deposition in the hole [Figs. 8(b) and 8(c)] gradually. To improve the welding area and the crown feature, a high-frequency laser wash procedure was then implemented on top of the
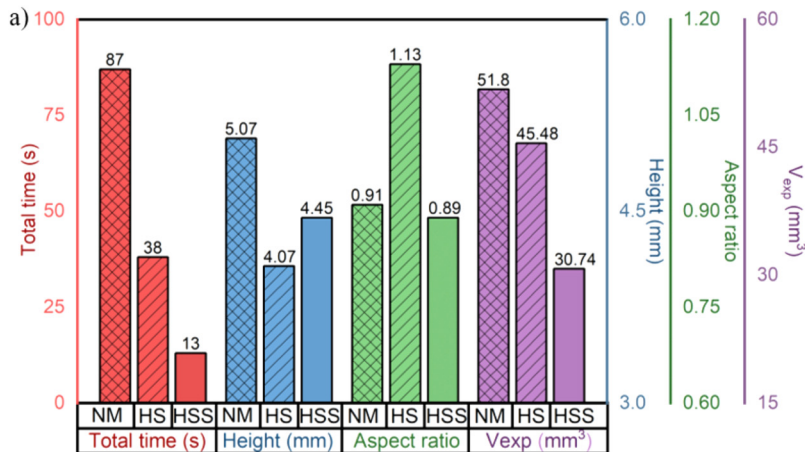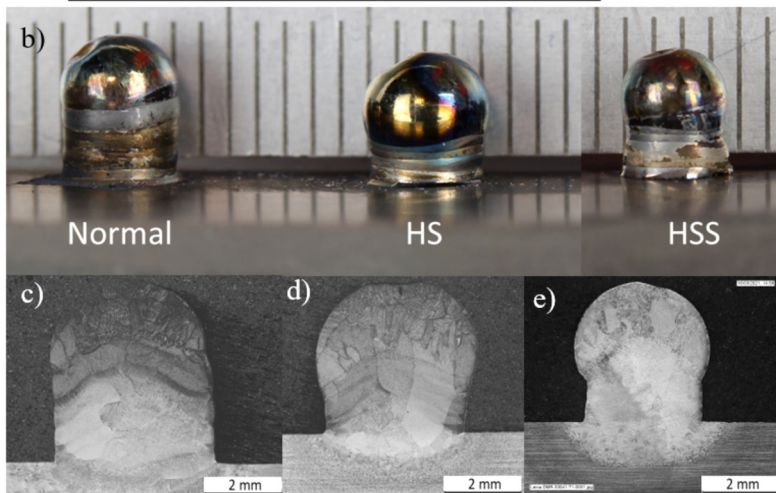
FIG. 7. Comparison of six-layer deposition built by three different LMWCD methods: (a) total processing time and geometrical dimensions; (b) outlook appearance; and their section microstructures of (c) NM, (d) HS, and (e) HSS methods.
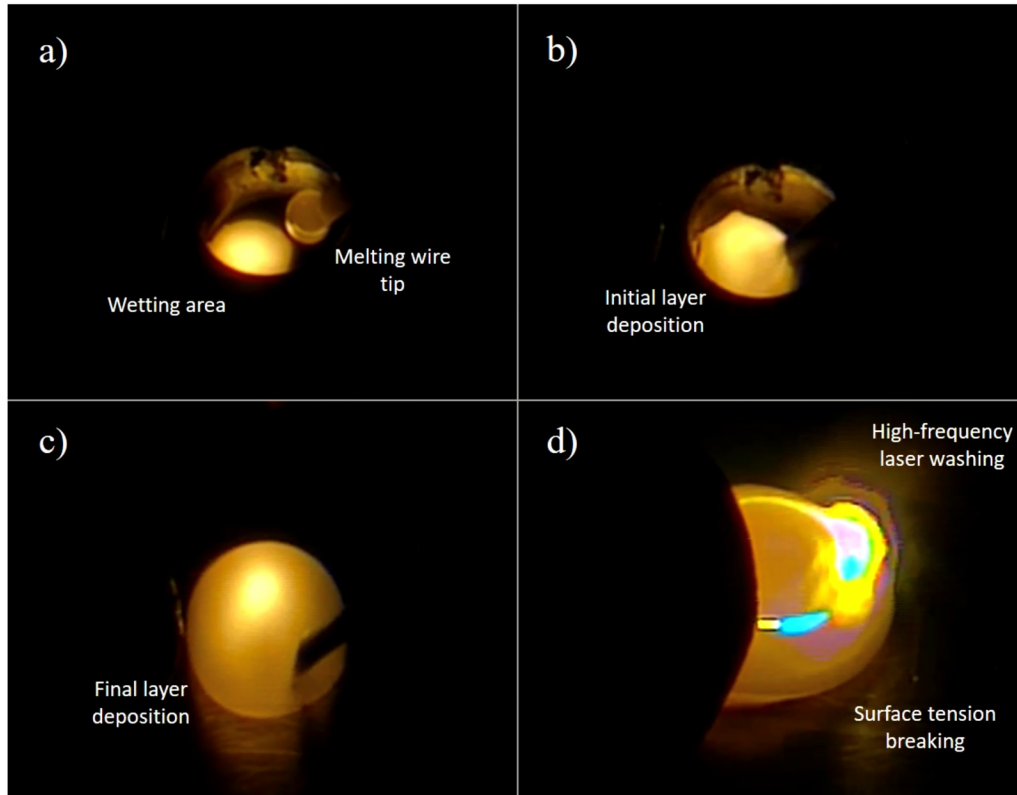
FIG. 8. Process recording of LR joining: (a) substrate surface prewetting, no deposit; (b) initial root deposition of the rivet, 1 mm deposition height; (c) rivet building at final circle layer, 6 mm deposition height; (d) postwash process on the top of the rivet, 5 mm final deposition height.

deposited rivet, shown in Fig. 8(d), and after a certain duration (e.g. 3–12 s), the surface tension on the top was broken and a new flatter crown was formed.

The geometrical results between the original and postprocessed rivets are illustrated in Figs. 9 and 10, which show the
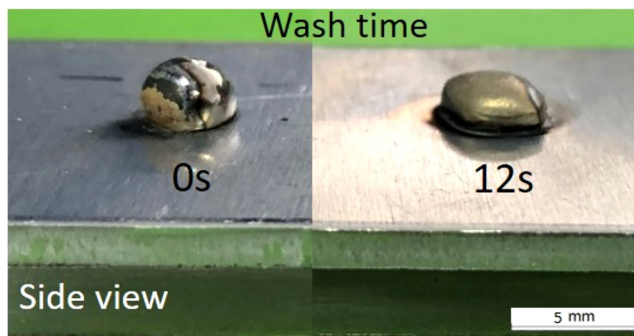

FIG. 9. Outlooks of rivers built by LR before and after 12 s laser washing postprocess.
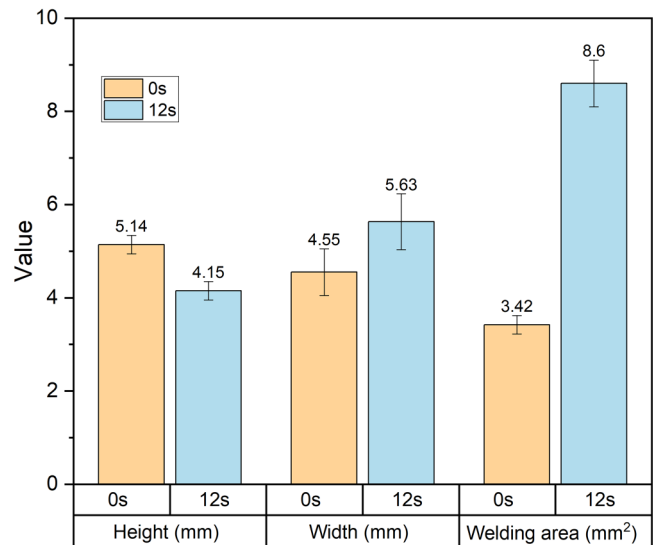

FIG. 10. Geometrical comparison results between original and postwashed rivets.

differences in the rivet height, diameter, and welded area between the rivet and the substrate. The flatter and larger diameter of the rivet crown after 12 s postwash not only interlocks the two joined sheets more properly but also provides a higher pulling strength for the joint with increased rivet diameter and contact in the joint.

The cross section views of the original and postwashed rivets are shown in Figs. 11(a) and 11(b) showing differences in the crown and weld. A prolonged period of laser scanning resulted in remelting of the originally deposited rivet. The combined effects of high-speed scanning melting the rivet deposit and gravity condensing the molten material resulted in the molten liquid flowing downward. This enlarged the welding area and reformed the geometrical shape of the rivet, resulting in a tighter fit onto the trunk (AA6061 upper sheet).

Due to the heat input and accumulation in the postwash process, the deposited rivet was completely remelted and partly diluted into the original fusion zone. The cross section views of the original and postwashed rivets are shown in Figs. 11(a) and 11(b) with clear differences in the crown and weld. The combined effects of high-speed scanning melting the rivet deposit and gravity condensing the molten material resulted in the molten liquid flowing downward. This enlarged the welding area and reformed the geometrical shape of the rivet, resulting in a tighter fit onto the trunk (AA6061 upper sheet). Near the weld area, larger HAZ and FZ areas were observed in Fig. 12(b), and the measured FZ depth was increased from $h_{FZ0} = 0.29$ mm in the original rivet to $h_{FZ1} = 0.73$ mm measured in the postwashed rivet. Moreover, the weld diameter was increased from $D_{w0} = 1.97$ mm in the original rivet to $D_{w1} = 3.05$ mm in the postwashed rivet; the corresponding welding area was expanded from 3.05 to 7.31 mm^2 by the postwashing process. Therefore, after the postwash process, the larger fusion zone and reformed rivet shape improved the welding
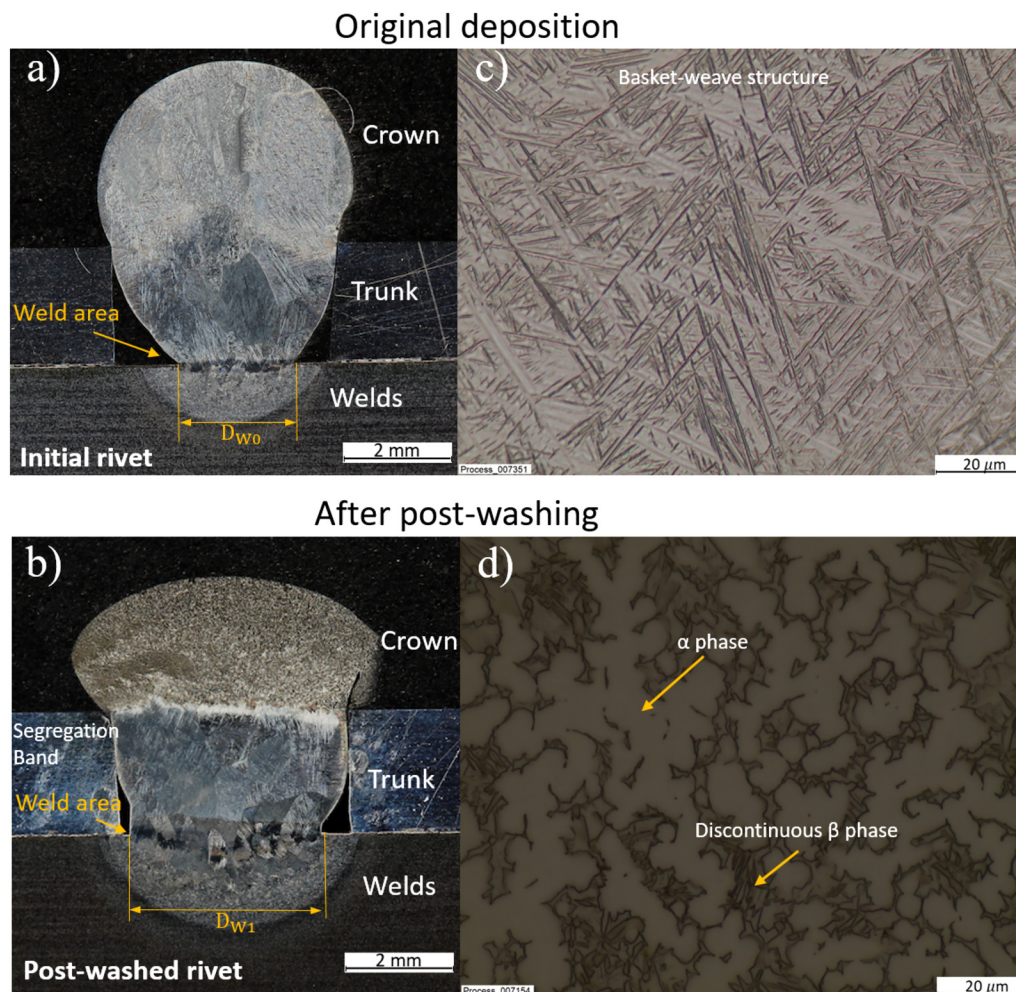

FIG. 11. Cross section overview of the (a) initial rivet and (b) postwashed rivet, and the microstructure map in the crown area of the (c) initial rivet and (d) postwashed rivet.
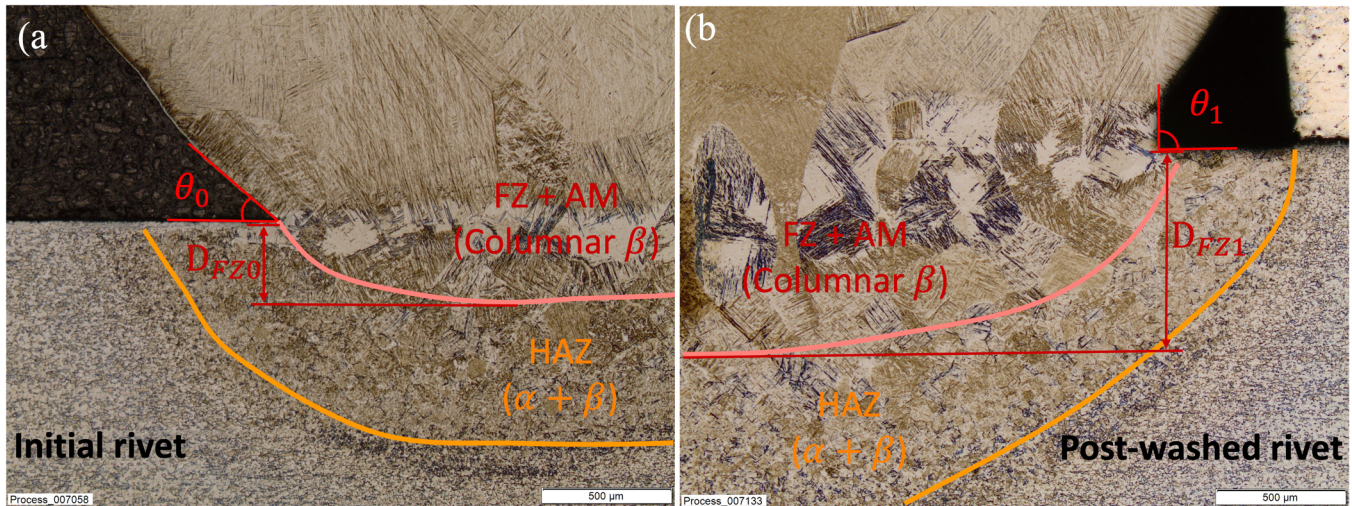
FIG. 12. Observation in the welding areas of the (a) initial rivet and (b) postwashed rivet.

area, which lead to enhanced shear and pulling strengths of the rivet.[28,29] From the multiple postwash trails on the original rivets, the average of welding diameter measured was 50.8% increased. In addition, compared to the original rivet in Figs. 12(a), the remelting process consolidated voids and gaps between the deposit and upper sheet are shown in Fig. 12(b), and the reformed deposition shape raised the deposition wetting angle θ. After the postwash, compared with the original rivet, the left wetting angle at deposition root was increased from $\theta_{l0} = 44°$ to $\theta_{l1} = 88°$, and the right angle was increased from $\theta_{r0} = 52°$ to $\theta_{r0} = 86°$ in the postwashed rivet, which improves the load-bearing condition.[30,31] For the microstructural comparison, HAZ depth and the number of columnar β were increased after the postwash; the deeper and denser grain boundaries might enhance the joining quality in this case as well.[32]

The microstructure of the original rivet shows a similar map with HSS deposition, and the regular Widmanstätten structure was observed on top of the deposition in higher magnifications in Fig. 11(c). However, it is worth noting that an obvious phase change occurred in the crown area of the postwashed rivet in Fig. 11(d), where plenty of dense primary-α-like grains were formed instead of the basket-weave structure. This is very rarely recorded in reports on LMWD research. One possible assumption is that the remelting status of the material had been maintained in the postscanning process and then followed with a slow air cooling from a high temperature (above 2000 °C) to the ambient one. This special thermal history caused the formation of the primary-α in the remelted crown. Another possible scenario is that a small part of the aluminum surface was cut by a high-velocity laser beam in the postscanning, the particles were splashed into the melt pool, and this increased the aluminum fraction in the material that enhanced the stabilization of the α phase.[33] There is a need for further metallurgic analyses and tests on these aspects.

The grain phase differences between the rivets without and with the postwash are also reflected in the microhardness curves in

Fig. 13. Due to the difference presented on the microstructure, the crown area of the postwashed rivet was measured with a higher hardness with an average of 750 HV1, which is 90% increased compared to the average of 395 HV1 in the unwashed rivet. In the laser wire deposition for the Ti6Al4V, grain boundaries and dislocation distribution of the α and β phase structures appeared in the microstructure dominantly influence the hardness;[34] therefore, the extremely higher value in the postwashed crown area is mainly because of the large crowded primary α grains formed.
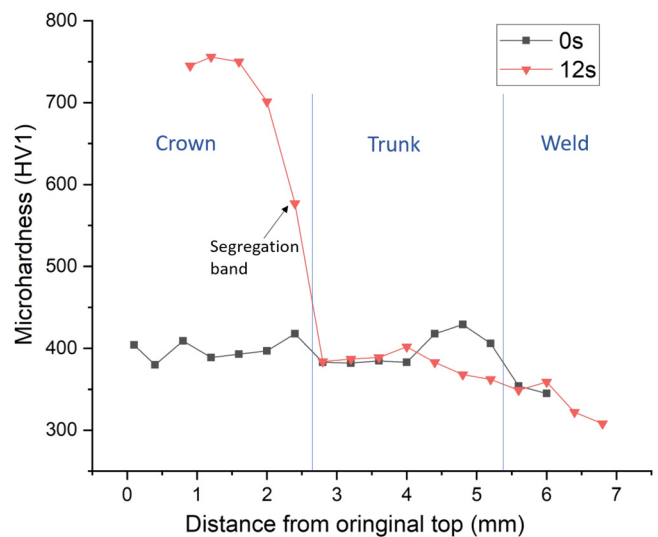

FIG. 13. Microhardness comparison results for the initial (0 s) and postwashed (12 s) rivets.

The unwashed rivet, however, presented a slightly higher hardness near the substrate surface due to a narrower welding area and columnar grain boundaries, which show an agreement with Ref. 15. Except the two locations discussed above, no obvious difference was found in other areas such as AM, HAZ, and BM, which were also consistent with the microstructure observations.

Because currently there is no commercial used titanium rivet for the dissimilar joining aim, instead, as one of the commonly used mechanical rivets in aerospace applications, a 4 mm 6 series blind rivet made of aluminum alloy body and carbon steel mandrel was selected for comparison.[35] The shear specimen's dimension is $125 \times 30\ mm^2$ with thicknesses of 2 mm and 4 mm, respectively, for the AA6061 upper sheet and Ti6Al4V substrate; the tests were conducted by Instron B910 and test velocity was set to 10 mm/min. The shear tests of unwashed, postwashed LR, and the blind rivet joints were carried out. The corresponding load-displacement curves are plotted in Fig. 14.

All of the rivets failed near the welding and connection area on the substrate surface where the shear force was primarily loaded. Because of the superior ductility of forged aluminum, the blind rivet showed the largest elongation (1.02 mm) compared to the two titanium LRs. However, for the peak shear strength, due to the higher strength of the Ti6Al4V alloy, the unwashed rivet also reached 1.28 kN, close to that of the blind rivet at 1.46 kN. Thanks to the enhanced thorough welding connection, the postwashed rivet gave the best overall performance, which not only presented a reasonably good ductility with 0.75 mm maximum displacement but also showed the highest peak shear load of 2.07 kN, with an increase of 61.7% and 41.8% compared to the unwashed LR and the blind rivet, respectively. The benefit of postwash was clearly demonstrated.

The microhardness of the original and postwashed rivets does not show a big difference because due to similar microstructures.
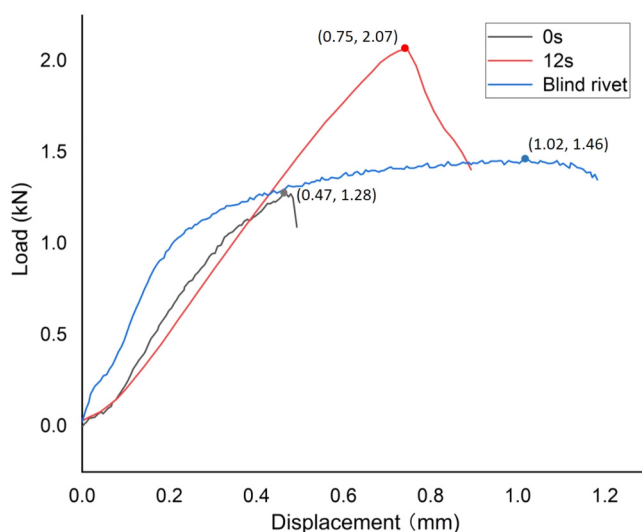

FIG. 14. Shear tests of 4 mm diameter unwashed, postwashed (12 s) LRs, and mechanical blind rivet.

As such, they should have a similar stress-strain curve at the welded location. However, the postwashed rivet has a larger welding area (Fig. 14); thus, in the load-deformation curve, the maximum shear load of the postwashed rivet is higher than that of the original rivet, in accordance to their welding areas.

IV. CONCLUSION

The feasibility study of LR has confirmed that the cylinder deposition can be built by the HSS method, and a proper cross section overview was observed in the microstructure without major defects such as porosity or cracks. The strength of the deposit was also tested by the microhardness measurements. Based on the study, the following conclusions can be drawn:

- Compared with the normal deposition method, the optimized HSS has a much higher productivity. It compresses the total process time from 87 to 13 s for a similar height feature, leading to improved productivity by 6.7 times.
- Energy input has a negative correlation with the deposition height but positive with the mass input.
- The postwash process improves the geometrical dimensions for both the crown and welding area of the rivet, leading to a large number of equiaxed α phases and increased microhardness.
- LR rivets provide comparable ductility and strength to a mechanically produced aluminum blind rivet, and the postwash process can help us to improve the strength by 62%.

REFERENCES

[1]X. Chen, Z. Lei, Y. Chen, M. Jiang, N. Jiang, J. Bi, and S. Lin, "Enhanced wetting behavior using femtosecond laser-textured surface in laser welding-brazing of Ti/Al butt joint," Opt. Laser Technol. **142**, 107212 (2021).

[2]A. H. Plaine, A. R. Gonzalez, U. F. H. Suhuddin, J. F. Dos Santos, and N. G. Alcântara, "The optimization of friction spot welding process parameters in AA6181-T4 and Ti6Al4V dissimilar joints," Mater. Des. **83**, 36–41 (2015).

[3]H. Zhao, M. Yu, Z. Jiang, L. Zhou, and X. Song, "Interfacial microstructure and mechanical properties of Al/Ti dissimilar joints fabricated via friction stir welding," J. Alloys Compd. **789**, 139–149 (2019).

[4]S. Chen, L. Li, Y. Chen, and J. Huang, "Joining mechanism of Ti/Al dissimilar alloys during laser welding-brazing process," J. Alloys Compd. **509**, 891–898 (2011).

[5]Y. Huang, J. Wang, L. Wan, X. Meng, H. Liu, and H. Li, "Self-riveting friction stir lap welding of aluminum alloy to steel," Mater. Lett. **185**, 181–184 (2016).

[6]H. Wang, X. Yuan, T. Li, K. Wu, Y. Sun, and C. Xu, "TIG welding-brazing of Ti6Al4V and Al5052 in overlap configuration with assistance of zinc foil," J. Mater. Process. Technol. **251**, 26–36 (2018).

[7]M. Geyer, V. Vidal, T. Pottier, C. Boher, and F. Rezai-Aria, "Investigations on the material flow and the role of the resulting hooks on the mechanical behaviour of dissimilar friction stir welded Al2024-T3 to Ti-6Al-4V overlap joints," J. Mater. Process. Technol. **292**, 117057 (2021).

[8]J. Mucha, "The failure mechanics analysis of the solid self-piercing riveting joints," Eng. Failure Anal. **47**, 77–88 (2015).

[9]M. Lißner, B. Erice, E. Alabort et al., "Multi-material adhesively bonded structures: Characterisation and modelling of their rate-dependent performance," Compos. Part B Eng. **195**, 108077 (2020).

[10]A. Pramanik, A. K. Basak, Y. Dong, P. K. Sarker, M. S. Uddin, G. Littlefair, A. R. Dixit, and S. Chattopadhyaya, "Joining of carbon fibre reinforced polymer (CFRP) composites and aluminium alloys—A review," Compos. Part A Appl. Sci. Manuf. **101**, 1–29 (2017).

[11]J. N. Zalameda, E. R. Burke, R. A. Hafley, K. M. Taminger, C. S. Domack, A. Brewer, and R. E. Martin, "Thermal imaging for assessment of electron-beam freeform fabrication (EBF3) additive manufacturing deposits," in *Thermosense: Thermal Infrared Applications XXXV*, 29 April–3 May 2013, Bellingham (International Society for Optics and Photonics, Baltimore, MD 2013), Vol. 8705, pp. 87050M.

[12]S. Liu, W. Liu, M. Harooni, J. Ma, and R. Kovacevic, "Real-time monitoring of laser hot-wire cladding of Inconel 625," Opt. Laser Technol. **62**, 124–134 (2014).

[13]W. E. Frazier, "Metal additive manufacturing: A review," J. Mater. Eng. Perform. **23**, 1917–1928 (2014).

[14]B. Baufeld, O. Van der Biest, and R. Gault, "Additive manufacturing of Ti–6Al–4V components by shaped metal deposition: Microstructure and mechanical properties," Mater. Des. **31**, S106–S111 (2010).

[15]E. Brandl, V. Michailov, B. Viehweger, and C. Leyens, "Deposition of Ti–6Al–4V using laser and wire, part I: Microstructural properties of single beads," Surf. Coat. Technol. **206**, 1120–1129 (2011).

[16]E. Brandl, V. Michailov, B. Viehweger, and C. Leyens, "Deposition of Ti–6Al–4V using laser and wire, part II: Hardness and dimensions of single beads," Surf. Coat. Technol. **206**, 1130–1141 (2011).

[17]A. G. Demir, "Micro laser metal wire deposition for additive manufacturing of thin-walled structures," Opt. Lasers Eng. **100**, 9–17 (2018).

[18]D. Ding, Z. Pan, D. Cuiuri, and H. Li, "Wire-feed additive manufacturing of metal components: Technologies, developments and future interests," Int. J. Adv. Manuf. Technol. **81**, 465–481 (2015).

[19]F. Khodabakhshi, M. H. Farshidianfar, S. Bakhshivash, A. P. Gerlich, and A. Khajepour, "Dissimilar metals deposition by directed energy based on powder-fed laser additive manufacturing," J. Manuf. Processes **43**, 83–97 (2019).

[20]X. Li, C. Pan, D. Fu, M. Wang, Z. Zhang, S. Qu, and C. Yang, "Fabrication of highly dissimilar TC4/steel joint with V/Cu composite transition layer by laser melting deposition," J. Alloys Compd. **862**, 158319 (2021).

[21]M. Mortello and G. Casalino, "Transfer mode effects on Ti6Al4V wall building in wire laser additive manufacturing," Manuf. Lett. **28**, 17–20 (2021).

[22]S. M. Kelly, "Thermal and microstructure modeling of metal deposition processes with application to titanium aluminum vanadium," Doctoral dissertation, Virginia Polytechnic Institute and State University, 2004.

[23]X. Bai, P. Colegrove, J. Ding et al., "Numerical analysis of heat transfer and fluid flow in multilayer deposition of PAW-based wire and arc additive manufacturing," Int. J. Heat Mass Transfer **124**, 504–516 (2018).

[24]B. Baufeld, E. Brandl, and O. Van der Biest, "Wire based additive layer manufacturing: Comparison of microstructure and mechanical properties of Ti–6Al–4V components fabricated by laser-beam deposition and shaped metal deposition," J. Mater. Process. Technol. **211**, 1146–1158 (2011).

[25]A. Ho, H. Zhao, J. W. Fellowes, F. Martina, A. E. Davis, and P. B. Prangnell, "On the origin of microstructural banding in Ti-6Al4V wire-arc based high deposition rate additive manufacturing," Acta Mater. **166**, 306–323 (2019).

[26]G. Lütjering and J. C. Williams, *Titanium*, Engineering Materials, Processes (Springer, Berlin, 2003).

[27]Y. Oshida, *Bioscience and Bioengineering of Titanium Materials* (Elsevier, New York, 2010).

[28]X. Sun, E. V. Stephens, and M. A. Khaleel, "Effects of fusion zone size and failure mode on peak load and energy absorption of advanced high strength steel spot welds under lap shear loading conditions," Eng. Failure Anal. **15**, 356–367 (2008).

[29]M. Pouranvari and S. P. H. Marashi, "Critical review of automotive steels spot welding: Process, structure and properties," Sci. Technol. Welding Joining **18**, 361–403 (2013).

[30]S.-H. Lin, J. Pan, S.-R. Wu, T. Tyan, and P. Wung, "Failure loads of spot welds under combined opening and shear static loading conditions," Int. J. Solids Struct. **39**, 19–39 (2002).

[31]J. H. Song and H. Huh, "Failure characterization of spot welds under combined axial–shear loading conditions," Int. J. Mech. Sci. **53**, 513–525 (2011).

[32]W. Xu, M. Brandt, S. Sun, J. Elambasseril, Q. Liu, K. Latham, K. Xia, and M. Qian, "Additive manufacturing of strong and ductile Ti–6Al–4V by selective laser melting via in situ martensite decomposition," Acta Mater. **85**, 74–84 (2015).

[33]A. Momeni and S. M. Abbasi, "Effect of hot working on flow behavior of Ti–6Al–4V alloy in single phase and two phase regions," Mater. Des. **31**, 3599–3604 (2010).

[34]D. Damisih, I. N. Jujur, J. Sah, and D. H. Prajitno, "Effect of heat treatment temperature on microstructure characteristic and hardness properties of casted Ti-6Al-4V ELI," Widyariset **4**, 153–162 (2018).

[35]G. Li, G. Renaud, and M. Liao, "Assessing the riveting process and the quality of riveted lap joints in aerospace and other applications," in *Welding and Joining of Aerospace Materials* (Woodhead Publishing, Cambridge, UK, 2021), pp. 383–426.